

Nanostructured zinc oxide gas sensors by successive ionic layer adsorption and reaction method and rapid photothermal processing

Oleg Lupan^{a,b}, Sergiu Shishiyanu^b, Lee Chow^{a,*}, Teodor Shishiyanu^b

^a Department of Physics, University of Central Florida, PO Box 162385 Orlando, FL, 32816-2385, USA

^b Department of Microelectronics and Semiconductor Devices, Technical University of Moldova, bd. Stefan cel Mare 168, FCIM, MD-2004, Chisinau, Republic of Moldova

Received 24 February 2007; received in revised form 20 October 2007; accepted 22 October 2007

Abstract

Undoped and Sn, Ni-doped nanostructured ZnO thin films were deposited on glass substrates using a successive ionic layer adsorption and reaction (SILAR) method at room temperature. The SILAR deposited zinc oxide films have been rapid photothermal processing (RPP) at various temperatures to study the effect of annealing on the sensing properties. Structural, electrical and sensing properties were investigated by means of X-ray diffraction (XRD), Energy Dispersive X-ray spectroscopy, scanning electron microscopy, electrical resistivity, and sensitivity measurements. Microstructures of the deposited films were studied for different concentrations of dopants and zinc-complex solution and temperatures. The results of influence of growth processes, doping, and RPP on phase structure, surface morphology, particles size and resistivity values are presented and discussed. The average grain size determined from XRD patterns was 240, 220 and 265 Å for ZnO, Sn–ZnO and Ni–ZnO films, respectively. Moreover, electrical characterization of the sensors prepared from SILAR deposited nanostructured zinc oxide thin film has been carried out. The variation in resistivity of the ZnO film sensors was obtained with doping and post-deposition rapid photothermal processing in vacuum and N₂ ambient. Electrical resistivity measurements showed semiconducting nature with room temperature resistivity 1.5 × 10⁵, 6.1 × 10², 70 Ω cm for as-deposited ZnO, 4 at.% Ni–ZnO and 4 at.% Sn–ZnO, respectively. These values decreased to 1 × 10⁴, 2 × 10², 30 Ω cm for RPP annealed films. The types of doping and temperatures of RPP were found to have an important role in determining the sensitivity and resolution of the NO₂, NH₃ ZnO-based sensors. While the nanostructured ZnO sensor showed higher ammonia sensitivity than that of NO₂, an enhanced NO₂ sensitivity was noticed with the ZnO films doped with 4 at.% Sn and higher NH₃ sensitivity was obtained by 4 at.% Ni doping of zinc oxide thin films.

© 2007 Elsevier B.V. All rights reserved.

Keywords: ZnO; SILAR; RPP; Sensor; Nanostructure

1. Introduction

The semiconductor zinc oxide is recognized as one of the most important semiconductor materials which exhibits numerous characteristics that may enable its efficient utilization for various technological applications such as antireflection coatings, transparent electrodes in solar cells [1,2], piezoelectric devices [3], varistors [4], surface acoustic wave devices [5], electro- and photoluminescent devices [6], gas sensors [7,8],

and others. Recently zinc oxide has attracted worldwide research interest because it is considered a promising material for thin film gas sensors in electronic noses [9,10]. Although ZnO is one of the earliest discovered semiconducting oxide gas sensing materials and there are many reports concerning the sensitivity properties of ZnO, most of these works has been done on powder samples usually pressed in pellets and sintered at high temperatures (900–1300 °C) [11,12]. In recent years, there appeared many publication on ZnO nanorod or thin film gas sensors using various synthesis techniques including molecular beam epitaxy [13–17], chemical vapor deposition [18,19], sputtering [20,21], thermal evaporation [22,23], and reactive vapor deposition [24].

* Corresponding author.

E-mail address: chow@ucf.edu (L. Chow).

However, only a few publications describe the sensing behavior of zinc oxide thin films deposited by aqueous solution techniques at low temperatures [25–28]. Unfortunately, they did not describe the impact of impurities, growth and annealing regimes on the film morphology and sensitivity of ZnO thin film based gas sensors.

The SILAR technique is a relative new and less investigated process reported by Nicolau [29]. As a method of thin film growth, SILAR is simple, flexible, and offers an easy way to dope film. It does not require high quality substrates, and can operate at room temperature without the need for vacuum. Besides it is also cost-effective and it can adapt to any substrate material (insoluble) or surface profile. Growth parameters are relatively easy to control and the stoichiometric deposit and different grain structures can be realized [27–31].

Semiconducting oxide sensors have been used for a few decades for low-cost detection of combustible and toxic gases. However, the sensitivity, selectivity, and stability have limited their use, often in favor of other more expensive gas detection instruments. Our recent investigation on SILAR grown doped nanostructured zinc oxide films, annealed by rapid photo-thermal processing (RPP) provide the opportunity dramatically increase the response of ZnO films, as their performance is directly related to exposed surface volume, electrical and sensitivity characteristics.

The investigation of SILAR and RPP as techniques for synthesis of sensor materials and the development of low-cost sensors for toxic NO₂ and ammonia will satisfy the need to monitor nitric oxides (NO and NO₂) in the exhaust gases from internal combustion engines, gas heating furnaces, which have large consequences on health and environmental pollution. Also the necessity for a NO_x/NH₃ sensor system in the fuel gas exhaust prior to the stack emission and a nitric oxide/ammonia sensor for fossil fuel combustion control applications is nowadays a very important target.

The present paper describes the effects of different dopants, and RPP temperature on structure and morphology and on the gas sensing characteristics of nanostructured ZnO thin films prepared by SILAR method. One of the advantages of the SILAR and RPP combination is that ZnO can be doped with different concentrations of Sn, Ni and rapid photothermal processed in different ambient for shorter durations (10–30 s) at lower temperatures (550–700 °C) than conventional furnace annealing (15–60 min at 700–1000 °C). Consequently, the sensitivity and selectivity of sensor elements could be investigated over a wide range of doping concentrations.

2. Experimental details

Films of pure ZnO and Sn, Ni-doped ZnO were deposited on Corning 7059 glass substrates by successive ionic layer adsorption and reaction method. This method is based on the adsorption and reaction of the ions from the aqueous solution at room temperature and rinsing between dippings, with de-ionized water (DI) in order to prevent homogeneous precipitation in the solution.

Before the growth process, the glass substrates were cleaned in dilute HCl (20%) solution for 10 min and then rinsed in DI water. Then the substrates were rinsed in ethanol acetone (1:1) mixture, DI water and dried in a nitrogen flux. Afterward the glass substrates exhibit hydrophilic property. Solutions of SnCl₂·2H₂O/HCl were used for the sensitization, because SnCl₂ dissolves in water and leaves Sn²⁺ in solution. This wets to the surface of the substrate and presents a “sensitized” surface for deposition. SnCl₂·2H₂O/HCl and PdCl₂/HCl solutions were used for the sensitization and activation, respectively. Throughout the growth process, the substrate was rinsed in de-ionized water (resistivity ~ 18 MΩ cm). The substrates were immersed vertically in the solutions.

The aqueous zinc-complex solution comprises a mixture of zinc sulfate (Zn(SO₄)·7H₂O), sodium hydroxide (NaOH) and sodium stannate (Na₂SnO₃·3H₂O), or nickel sulfate mixed until complete dissolution. The concentration of complex solution was diluted to obtain 0.08 M and 0.12 M zinc concentration for deposition by adding respective quantities of DI water according to results of preliminary investigations. Adding the sodium stannate in the aqueous solution 5 at.% (and 7 at.%) Sn concentration, or nickel sulfate (NiSO₄·6H₂O) 4 at.% (and 6 at.%) Ni concentration according to doping level. The complex solution of cations was kept at room temperature and the aqueous solution of anions was kept at 95–98 °C during deposition. Nanostructured ZnO films growth by SILAR method comprised four steps for a full growth cycle. First the substrate was immersed in aqueous zinc-complex solution for 5 s, and then rinsed in DI water for 10 s to remove loose and excess zinc-complex ions. Then the substrate was reacted with anions from anionic precursor aqueous solution at 95–98 °C for 5 s, and ZnO is formed on the interface. In the last step the excess, unreacted species and the reaction byproduct are removed by washing the substrate for 10 s in DI water. The deposition cycles were repeated until the desired thickness was obtained according to growth kinetics previously studied in [30,31]. The as-deposited ZnO thin films were dried in air at 150 °C for 5 min. The details of tin-doped zinc oxide films deposited by the SILAR method were reported previously [30,31].

In order to investigate the effect of post-deposition annealing, films have been rapid photothermal processed at temperatures 300–750 °C in a low vacuum (10⁻¹ Pa) and N₂ ambient using an IFO-6 RPP system [30,32]. The duration of RPP was 20 s and the temperatures 550 and 650 °C for Ni and Sn-doped ZnO films, according to previously investigation results and reports [27,30,31]. The schedules of the RPP processed pure ZnO, and tin or nickel-doped zinc oxide thin film based sensor elements are summarized in Table 1.

The phase structure of these deposited films were studied using Rigaku X-ray diffractometer (XRD) model ‘D/B max’ equipped with a high-intensity CuK_α radiation (λ = 1.54178 Å) and optimized operating conditions of 30 mA and 40 kV at a scanning rate of 0.04°/s in the 2θ range of 10–90°. The composition and morphologies of ZnO films were characterized by Rutherford Back Scattering (RBS) spectroscopy, energy dispersion X-ray (EDX) spectroscopy and scanning

Table 1
The schedules of ZnO, Sn–ZnO, Ni–ZnO film based sensor samples RPP processing

RPP regimes	Sensor element								
	1.1 (ZnO)	2.1 (Sn–ZnO)	3.1 (Ni–ZnO)	1.2 ZnO	2.2 Sn–ZnO	3.2 Ni–ZnO	1.3 ZnO	2.3 Sn–ZnO	3.3 Ni–ZnO
Duration of RPP (s)	As grown	As grown	As grown	20	20	20	20	20	20
Temperature of RPP (°C)	–	–	–	550	550	550	650	650	650

electron microscope (SEM). The RBS measurements were carried out with a 2.05 MeV He 2+ beam using a General IONEX 1.7MV Tandetron accelerator. The SEM and EDX was carried out using a VEGA TS 5130MM, 20 keV scanning electron microscope equipped with an Energy Dispersive X-ray (EDX) spectrometer for chemical composition microanalysis. Despite the relatively low growth temperature and short duration of the rapid photothermal annealing, the Zn and O content in the films was 1:1 within the experimental accuracy of the two techniques. These investigations confirmed that these films are polycrystalline with regular shaped particles with grains and pores distributed throughout the film surface. These films morphology are considered to play a vital role in the process of gas absorption and hence influence the sensitivity of the sensors. After RPP of zinc oxide thin films at 550 and 650 °C for 20 s in the N₂ ambient or in vacuum, the Al electrodes were deposited on to the surface in vacuum system. The electrical characterization was performed using two-point probe method in the temperature range of 300–600 K. The *n*-type of conductivity exhibited by zinc oxide films was confirmed by using an Ecopia Hall effect measurement system.

The sensor studies were performed in a closed quartz chamber connected to a gas flow system described in [31,33]. The concentration of test gases NO₂ or ammonia was measured using pre-calibrated gas flow meters. The temperature of the thin film sensor element was controlled between room temperature and 250 °C. A computer with suitable interface handled all controls and acquisition of data.

3. Results and discussions

3.1. Structural analyses

Fig. 1 shows the XRD diffraction pattern of the (a) pure, (b) Ni-doped, and (c) Sn-doped ZnO films. The diffraction peaks in the pattern can be indexed to hexagonal wurtzite structured ZnO (space group: P6₃mc(186); *a*=0.3249 nm, *c*=0.5206 nm) and diffraction results are in agreement with JCPDS card for ZnO (JCPDS 036-1451) [26]. The intensity of the peaks relative to the background signal demonstrates hexagonal phase of the products and high crystallinity of the ZnO samples grown by SILAR. The characteristic peaks of Zn(OH)₂ was not observed, which indicated a single phase hexagonal ZnO. The nanocrystallites are oriented along the *c* axis, [002] direction. The doping with Ni (Fig. 1b) seems to take place through substitution of Zn cations by Ni ions, because the modification of ZnO crystal structure was minimum. The doping of Sn (Fig. 1c) on the other

hand seems to be problematic due to the appearance of two new peaks of SnO₂(200) and SnO(102). Also these diffraction results (Fig. 1b and c) are in agreement with JCPDS cards (JCPDS 072-1464, and 024-1470, 041-1445), respectively [34].

The mean grain size (*d*) of the ZnO nanostructured samples, were calculated using Scherrer's equation:

$$d = \frac{K\lambda}{(\beta^2 - \beta_0^2)^{1/2}} \cos \theta \quad (1)$$

where β is the measured broadening of a diffraction line peak, full width at half its maximum intensity in radians, β_0 — the instrumental broadening, $K = 180/\pi$, λ is the X-rays wavelength (0.154056 nm) and θ is the Bragg diffraction angle. The average grain size determined from XRD patterns was 240, 220 and 265 Å for ZnO, Sn–ZnO and Ni–ZnO films, respectively.

For surface morphology and estimation of the film thickness, SEM technique has been used. Using EDX and RBS, the formation of the ZnO and the doping with Sn and Ni in ZnO was confirmed.

Fig. 2 shows SEM secondary electron images of the undoped and Sn, Ni-doped ZnO films on glass substrate corresponding to sensor samples (1.1, 1.3, 2.3 and 3.2) described in Table 1, respectively. It can be observed that the

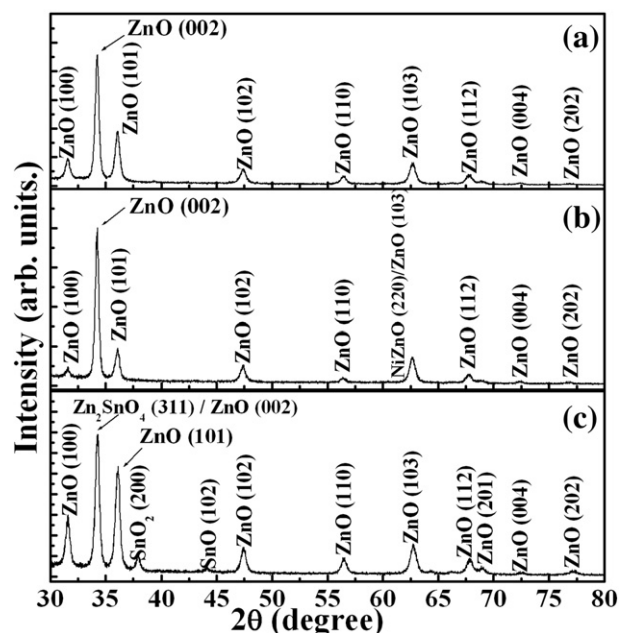


Fig. 1. The XRD pattern of the ZnO films: (a) undoped, (b) Ni-doped, and (c) Sn-doped obtained by SILAR method.

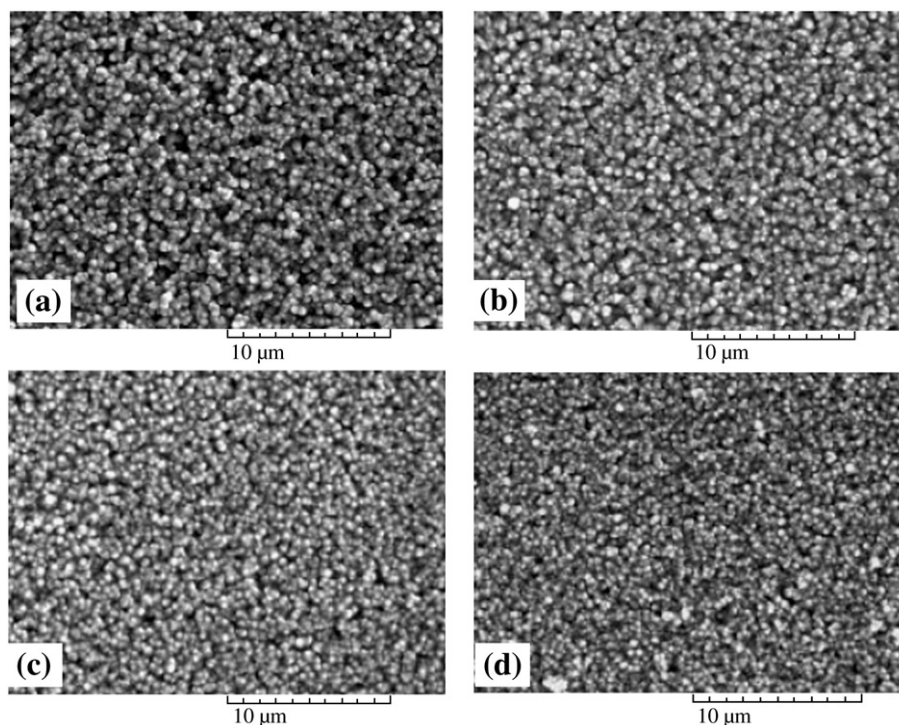


Fig. 2. SEM secondary electron images of the pure and the doped ZnO films onto glass substrates (corresponding to Table 1) showing the influence of dopant and annealing on surface morphology: (a) undoped as-grown film, (sample 1.1), (b) undoped after RPP 650 °C, 20 s, (sample 1.3), (c) tin-doped Sn/Zn, after RPP 650 °C, 20 s, (sample 2.3), (d) nickel-doped Ni/Zn after RPP 550 °C, 20 s, (sample 3.2). The scale bars are 10 μm long.

surface morphology to the films is dependent on the type of the dopant atoms (Sn or Ni), Fig. 2c and d. The crystallites of the SILAR grown films are visible and have the mean sizes around 400, 200 and 150 nm for ZnO, Sn–ZnO and Ni–ZnO films, respectively. For the estimation of a mean crystallites size for the films, we drew a line on the SEM image and divided the length by the number of grain boundaries crossing the line.

The impact of the rapid photothermal processing on the surface morphology of the deposited films has also been investigated. In the 150–350 °C RPP temperature range the films surface morphology do not differ from the as-grown ZnO

(Fig. 2a) which appeared to have voids and was intentionally omitted. Increasing the RPP temperature up to 550 °C for Ni-doped and up to 650 °C for pure and Sn-doped zinc oxide decreases the voids in the film (Fig. 2b,c and d, respectively). In Fig. 2b the micrograph of the ZnO films RPP processed at 650 °C, 20 s appeared to be more dense than Fig. 2a.

The SEM images of as-grown, Sn-doped ZnO films do not differ from that rapidly annealed at various temperatures (300–700 °C) shown in Fig. 2c. There is no difference in the shape of the grains of ZnO–Ni treated by RPP. As is evident in Fig. 2d, the ZnO–Ni films show smaller grains than pure ZnO.

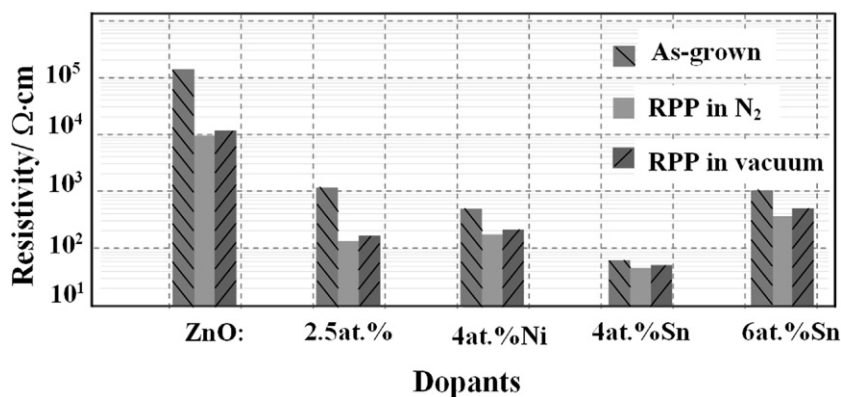


Fig. 3. Electrical resistivity values versus dopant concentration of the different ZnO films as-grown and after RPP in vacuum or N₂ ambient. ZnO and Sn–ZnO films were subjected to rapid photothermal processing at 650 °C; Ni–ZnO was subjected to RPP at 550 °C for 20 s.

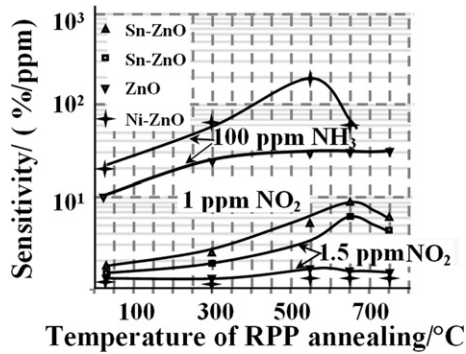


Fig. 4. The sensitivity of the ZnO sensor as function of RPP annealing temperatures towards 1 ppm NO₂ and 100 ppm NH₃.

The Sn/Zn and Ni/Zn ratios in films was analyzed by EDX measurement and was found to be less than that in the solution; nevertheless, it was determined a linear correlation between both quantities. The Sn/Zn and Ni/Zn ratios surveyed are 4/96 and 2.5/97.5 (at.%) in different scanned regions on samples of set 2 (5 at.% Sn) and set 3 (4 at.% Ni), respectively.

3.2. Electrical properties

The pure ZnO films have lower stability in corrosive, humid ambient due to large amount of O vacancies [35]. The properties of such zinc oxide films are often altered by adsorption of CO₂, O₂, and water. Therefore SILAR grown ZnO film have been doped with Sn, Ni to modify and enhance their properties. Fig. 3 show the electrical resistance of the undoped, Sn and Ni doped ZnO thin films versus RPP temperature performed using two point probe method.

The electrical resistance decreases with doping with elements Sn, Ni and with rapid photothermal processing temperature up to 650 °C and take place simultaneously with the elimination of voids inside the pure and doped-ZnO films.

Irreversible changes in the electrical characteristics have been observed when the ZnO films were post-growth rapid photothermal processed at temperatures higher than 300 °C for 20 s duration. In the temperature range of 550–650 °C, improvement of the quality and stability of the ZnO sensor samples has been observed. The measurement has been carried out during one year and it was determined that the doped ZnO-based sensor elements have higher conductance stability, which ensures a stable zero level for gas sensor applications.

3.3. Gas sensing properties

For gas sensing characterisations, the sensor elements were placed in a 1000 cc gas chamber. The undoped, Sn and Ni doped zinc oxide films were used to detect NO₂ and ammonia at room temperature and up to 250 °C in the concentrations of 1–1.5 ppm and 100 ppm, respectively. The readings were taken 20 min after the gases have been introduced in the test chamber. It was found that resistance change $\Delta R = |R_{\text{gas}} - R_{\text{air}}|$ increased with gas concentration.

The sensitivity of the sensor element to gases was calculated according to the formula [30,36]:

$$S = \frac{100 \cdot (|R_{\text{gas}} - R_{\text{air}}|)}{C \cdot R_{\text{air}}}, \quad (2)$$

where C is the gas concentration, R_{gas} and R_{air} are the electrical resistance of the sensor element in the presence of gas and in air, respectively.

The sensitivity to 1.0 and 1.5 ppm NO₂ and 100 ppm ammonia of the ZnO, Ni-ZnO and Sn-ZnO elements are shown in Fig. 4 as a function of temperature of RPP annealing. The sensitivity increased with increasing RPP temperature and attained a maximum to NH₃ at about 550 °C for Ni-ZnO and to NO₂ at about 650 °C for *n*-ZnO and Sn-ZnO. The resistivity on the other hand, was not restored to the original level within 60 min for sensors RPP below 400 °C, 20 s. Therefore, was demonstrated that RPP temperature in the range 550–650 °C and duration 20 s was desirable for these elements from the viewpoints of sensitivity.

The magnitude of the NO₂ response is increased for Sn-doped ZnO films grown by SILAR and RPP. The films shown in Fig. 2c and d are from a morphological point of view similar, but have quite different responses to NO₂. A similar effect was observed for samples with Ni-doped ZnO thin films RPP at 550 °C, 20 s (Fig. 4) where the ammonia response is higher.

n-type ZnO films sensitivity can be explained by a drop in the oxygen partial pressure which is associated with a variation of the sensor baseline resistance. The presences of reducing gases (ammonia) influence in the same manner the sensor resistance due to a decreasing of the oxygen on the surface and as a result reduce sensor resistance. Oxidizing gases (NO₂) increase the resistance by increasing the coverage of ion-sorbed oxygen [37].

A typical calibration curve of sensor is presented in Fig. 5 and shows the sensitivity of the nanostructured zinc oxide sensor element measured against increasing NO₂ gas concentration at 20 °C and 150 °C. It was observed that the 4 at.% Sn-ZnO sensor exhibits greater sensitivity to 1 ppm NO₂ at 150 °C. The linear detection range from 0.5 to 1.0 ppm was obtained for sensor with 4 at.% Sn-ZnO RPP at 650 °C for 20 s operated at

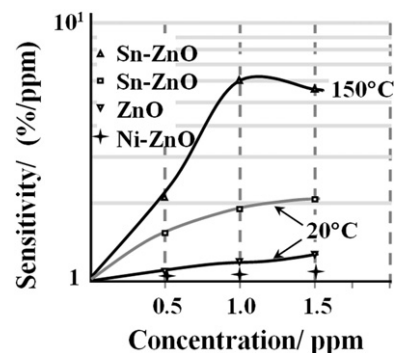


Fig. 5. The sensitivity change of the ZnO sensor elements against increasing gas concentration at room temperature (20 °C) and at operating temperature 150 °C.

150 °C. These results ensure application of this method to develop a nanostructured ZnO sensor to detect NO₂ at low ppm range (0.5–1.0 ppm).

A certain degree of selectivity can be realized by controlling the operating temperature [38] when sensing film is sensitive to several gases. The sensitivity of nanostructured ZnO gas elements is relatively high and is related to the grain size effect [39].

For the pure ZnO sensor, the resistance was quite high (10⁵ Ω cm in air and over 10⁶ Ω cm in 1.5 ppm NO₂) and the response time to NO₂ and ammonia was quite slow. It appears that due to leakage current in the circuit, the data were un-reliable and the applicable electrical parts are restricted. By introducing Ni, Sn dopants into the ZnO film sensor, we reduce the resistance and change the sensor characteristics, such as selectivity, sensitivity and long-term stability. The best performance have been obtained using a Sn-doped ZnO thin film, rapid photothermal processed at 650 °C for 20 s and at an operating temperature of 150 °C. Fig. 6 shows the 4 at.% Sn–ZnO sensors dynamic response to 1 ppm NO₂. The response and recovery times of the sensor (time for 90% of total conductance change) for 1 ppm NO₂/dry air mixture were about 20 and 25 min, respectively. The sensitivity defined according to experimental results (Fig. 6) was 9%/ppm and is attractive for practical sensor applications. The sensor showed relatively fast response and baseline recovery for 1 ppm NO₂ detection.

The NH₃ sensing characteristics of sensors were performed in a dry atmosphere. Fig. 7 shows the response kinetics of 4 at.% Ni-doped ZnO sensor annealed by RPP at 550 °C, 20 s towards 100 ppm concentration of ammonia pulse at room temperature. From Fig. 7 we can see the response of the sensor to ammonia is quite fast for the annealed sample, but the saturation time is different for adsorption and desorption processes. The results for samples processed at temperature below 500 °C is omitted due to instability of the kinetics of response in these sensor elements.

The typical response times for the pure and Ni-doped ZnO sensors have been found to be 20 and 1 min, respectively. The faster response of the Ni-doped ZnO sample is believed to be due to the fact that Ni doping creates high porous sensing ZnO films

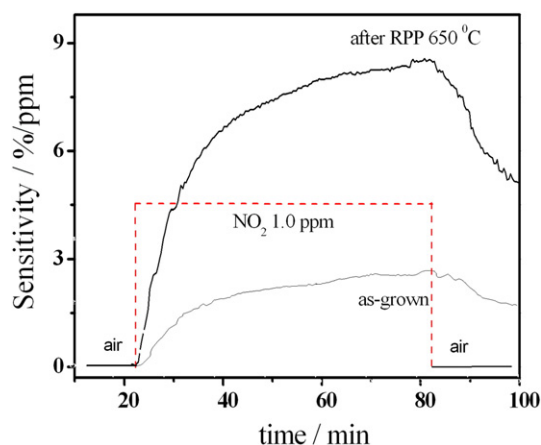


Fig. 6. The response time of a Sn-doped ZnO based sensor operated at 150 °C towards 1 ppm NO₂.

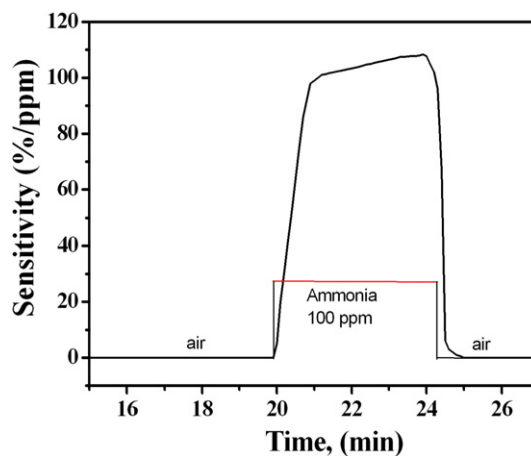


Fig. 7. The response time to 100 ppm NH₃ of the gas sensor based on Ni-doped ZnO film that was RPP at 550 °C for 20 s.

with smaller granule. This porous nature was confirmed by SEM images (Fig. 2d) and show higher surface-to-volume ratio of nanostructured films. Response kinetics studies on several sensors confirm that the Ni-doped ZnO thin film samples demonstrate sharper response and short recovery times. Surface defects and configuration seems to play a key role on the detection. For instance, it has been observed that high annealing temperature leads to better NO₂ sensor response, despite grain size increase in the SILAR gas sensors based on ZnO thin films.

Fig. 7 shows that sensor response and recovery time constants are on the order of 30 s, but after 60 s the signal becomes pretty stable. The conductivity decreased rapidly by exposing the sensor to ammonia, and recovered toward the original value after introducing clean air.

These results on SILAR gas sensors with Sn and Ni-doped ZnO films obtained in this work are superior to ZnO-based sensors reported in previous studies [27,30,31]. Also they offer possibility to integrate NO₂ and ammonia sensors on the same substrate using two different regions of ZnO sensing film.

4. Mechanisms for sensing

We use a phenomenological expression [40,41] to describe the conductivity (σ) of zinc oxide as follow

$$\sigma = \sigma_0 \exp\left(-\frac{E_A}{kT}\right) p(O_2)^{\frac{1}{m}} \quad (3)$$

where k is Boltzmann's constant, T temperature in Kelvin. The value of m is strongly dependent on the nature of the predominant defects involved in conduction mechanism. The activation energy E_A is the sum of thermal activation energy of charge carriers and energy necessary to form the defects. Doping of ZnO produces the electronic defects and increases the influence of oxygen partial pressure $p(O_2)^{\frac{1}{m}}$ on the conductivity of the films.

The gas response of Sn-doped ZnO sensors operated at temperature ~ 150 °C is controlled by the surface reaction. The concentration of species O_2^- , O^- is changed by the chemisorption.

Thus an oxygen ion acts as a trap for electrons from the bulk of the films. The electrons are taken from ionized donors through conduction band and the density of majority charge carriers at the gas–solid interface is reduced. This leads to the formation of a potential barrier for electrons with increasing of the oxygen ions density on the surface the further oxygen adsorption is inhibited. Thus at the junctions between ZnO grains, the depletion layer and potential barrier leads to the increasing of the electrical resistivity value. This value is strongly dependent on the concentration of adsorbed oxygen ions of the surface. Introducing the *n*-ZnO films in an NO₂ ambient will change the concentration of these ions and increase the resistance. The reaction in an NO₂ oxidizing gas:



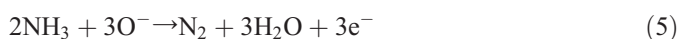
will lead to the consumption of electrons and increase the potential barrier height and of resistivity.

The surface reaction processes can explain the sensing mechanism to ammonia. The surface adsorbs H₂O in the air and upon exposure to ammonia a surface reaction take place with physisorbed H₂O. The resulted reaction product NH₄OH that is volatile in nature may cause decreasing of the conductivity and increasing sensitivity [42].

The negligible quantity of the surface reaction product and its high volatility indirectly indicates the observed quick response of the Ni–ZnO sensor to ammonia and quick recovery to initial conditions. The observed sensitivity variations of ZnO and Sn–ZnO sensor elements also may be attributed to the crystallite size variation in the films.

The ammonia molecule is firstly adsorbed on a Ni–ZnO surface. As soon the ammonia molecule is adsorbed, it can hop on the surface and thus undergo different processes. If it is not simply desorbed, the next step is its dehydrogenation through an oxygen species, which capture the hydrogen atom to form a hydroxyl group. This process leads to the formation of NH_x species. These species are no longer/likely to be desorbed but to further react following two main paths. They can interact with a second NH_x species to form molecular nitrogen (N₂). The second option is that NH_x species react with an oxygen centre (either chemisorbed or lattice oxygen) to form nitrogen monoxide (NO) [41,42]. The Ni–ZnO shows the higher sensitivity to NH₃ has smallest crystallite size when compared to the ZnO, Sn–ZnO based sensors as is observe in the SEM images Fig. 2d.

The improvement of sensor response obtained by the addition of catalytic additives was expected to promote a more selective catalytic oxidation of ammonia in order to avoid undesired reaction products (e.g. NO) and they should consume more oxygen species. The selective oxidation of ammonia should ideally lead to nitrogen, but other option is the formation of N₂O by internal selective catalytic oxidation. Gas sensors based on ZnO have typically a low sensor response to nitrogen oxide and so it cannot be considered that this gas would interfere on sensor response. Regarding to the enhancement of sensor response, the additives used (nickel ions) are undergo redox processes through the well-known Mars and van Krevelen (MvK) mechanism [38].



Increasing of charge carriers' concentration in the films is manifested by resistivity reduction according to our experimental results.

5. Conclusion

In this study the structures on the nanostructured ZnO:Sn, ZnO:Ni films as a nitrogen dioxide and ammonia gas sensors obtained by SILAR and RPP were investigated. The merit of this technology is in simplicity of the process, economy in energy, structures with high efficiency, short duration, energy save, accessible auxiliary materials and nonsophisticated equipment. We can easily modify electrical, morphological and sensing properties of zinc oxide films by controlling growth regimes, doping and RPP treatment conditions.

We have demonstrated the Sn doped ZnO thin film sensor toward NO₂ gas and Ni-doped ZnO to ammonia. It was shown that undoped ZnO thin films have a very low sensing response towards NO₂ and ammonia. The gas sensing characteristics of the ZnO films can be improved drastically by introducing tin (nickel) dopants into the sensing films. The sensitivity is higher for sensor elements on the Ni–ZnO and Sn–ZnO rapid photo-thermal processed at 550 °C and 650 °C, 20 s, respectively. The effects of doping with Ni, Sn on gas sensitivity should be related with such changes in morphology, but are necessary further investigations to determine the mechanisms. We continue investigations with different dopants and second components in ZnO films obtained by SILAR and RPP techniques.

Acknowledgements

The research described in this publication was made possible in part by Award No. MTFP-1014B of the Moldovan Research and Development Association (MRDA) under funding from the U.S. Civilian Research and Development Foundation (CRDF).

We would like to thank the help of Prof. Dr.hab. I. Tigineanu, Mr. Monaico E., National Center for Materials Study and Testing, for the SEM, EDX analyses, and Prof. Dr. Hab. D. Tsiulyanu, Technical University of Moldova, for sensing characteristics measurements.

Financial support by the Project 321b/s from the Ministry of Education and Science of Moldova and Project 032P from Supreme Council for Research and Technological Development of the Academy of Sciences of Moldova are gratefully acknowledged.

References

- [1] T. Ootsuka, Z. Liu, M. Osamura, Y. Fukuzawa, R. Kuroda, Y. Suzuki, N. Otagawa, T. Mise, S. Wang, Y. Hoshino, Y. Nakayama, H. Tanoue, Y. Makita, *Thin Solid Films* 476 (2005) 30.
- [2] R.R. Potter, *Sol. Cells* 16 (1986) 521.
- [3] S.C. Ko, Y.C. Kim, S.S. Lee, S.H. Choi, S.R. Kim, *Sens. Actuators, A* 103 (2003) 130.
- [4] J.H. Han, D.Y. Kim, *J. Europ. Ceram. Soc.* 18 (1998) 765.
- [5] S.H. Seo, W.C. Shin, J.S. Park, *Thin Solid Films* 416 (2002) 190.
- [6] A. Mitra, R.K. Thareja, V. Ganesan, A. Gupta, P.K. Sahoo, V.N. Kulkarni, *Appl. Surf. Sci.* 174 (2001) 232.

- [7] D.H. Yoon, G.M. Choi, *Sens. Actuators, B* 45 (1997) 251.
- [8] S.Y. Sheng, Z.T. Shu, *Sens. Actuators, B* 12 (1993) 5.
- [9] H.K. Hong, C.H. Kwon, S.R. Kim, D.H. Yun, K. Lee, Y.K. Sung, *Sens. Actuators, B* 66 (2000) 49.
- [10] T. Hofmann, P. Schieberle, C. Krummel, A. Freiling, J. Bock, L. Heinert, D. Kohl, *Sens. Actuators, B* 41 (1997) 81.
- [11] J. Xu, Q. Pan, Y. Shun, Z. Tian, *Sens. Actuators B* 66 (2000) 277.
- [12] J.D. Choi, G.M. Choi, *Sens. Actuators, B* 69 (2000) 120.
- [13] L.C. Tien, P.W. Sadik, D.P. Norton, L.F. Voss, S.J. Pearton, H.T. Wang, B.S. Kang, F. Ren, J. Jun, J. Lin, *Appl. Phys. Lett.* 87 (2005) 222106.
- [14] H.T. Wang, B.S. Kang, F. Ren, L.C. Tien, P.W. Sadik, D.P. Norton, S.J. Pearton, J. Lin, *Appl. Phys. Lett.* 86 (2005) 243503.
- [15] B.S. Kang, Y.W. Heo, L.C. Tien, D.P. Norton, F. Ren, B.P. Gila, S.J. Pearton, *Appl. Phys. A* 80 (2005) 1029.
- [16] H.T. Wang, B.S. Kang, F. Ren, L.C. Tien, P.W. Sadik, D.P. Norton, S.J. Pearton, J. Lin, *Appl. Phys. A* 81 (2005) 1117.
- [17] B.S. Kang, H.T. Wang, L.C. Tien, F. Ren, B.P. Gila, D.P. Norton, C.R. Abernathy, J. Lin, S.J. Pearton, *Sensors* 6 (2006) 643.
- [18] Z. Fan, J.G. Lu, *Proceeding of the 5th IEEE Conference on Nanotechnology*, Nagoya, Japan, July 11–15, 2005, p. 403.
- [19] S. Basu, A. Dutta, *Mater. Chem. Phys.* 47 (1997) 93.
- [20] H. Gong, J.Q. Hu, J.H. Wang, C.H. Ong, F.R. Zhu, *Sens. Actuators B* 115 (2006) 247.
- [21] J.X. Wang, X.W. Sun, Y. Yang, H. Huang, Y.C. Lee, O.K. Tan, L. Vayssieres, *Nanotechnology* 17 (2006) 4995.
- [22] Q. Wan, Q.H. Li, Y.J. Chen, T.H. Wang, X.L. He, J.P. Li, C.L. Lin, *Appl. Phys. Lett.* 84 (2004) 3654.
- [23] T. Gao, T.H. Wang, *Appl. Phys. A* 80 (2005) 1451.
- [24] L. Liao, H.B. Lu, J.C. Li, H. He, D.F. Wang, D.J. Fu, C. Liu, W.F. Zhang, *J. Phys. Chem. C*, 111 (2007) 1900.
- [25] A.P. Chatterjee, P. Mitra, A.K. Mukhopadhyay, *J. Mater. Sci.* 34 (1999) 4225.
- [26] P. Mitra, A.P. Chatterjee, H.S. Maiti, *Mater. Lett.* 35 (1998) 33.
- [27] O. Lupan, *J. Meridian Engineering* 3 (2004) 41 (ISSN-1683-853X).
- [28] T.P. Niesen, M.R. De Guire, *J. Electroceram.* 6 (2001) 169.
- [29] Y.F. Nicolau, *Appl. Surf. Sci.* 22–23 (1985) 1061.
- [30] S.T. Shishiyanu, T.S. Shishiyanu, O.I. Lupan, *Sens. Actuators, B* 107 (2005) 379.
- [31] O. Lupan, Ph.D. Thesis, Technical University of Moldova, Republic of Moldova, 2005.
- [32] S.T. Shishiyanu, O.I. Lupan, E. Monaico, V.V. Ursaki, T.S. Shishiyanu, I.M. Tiginyanu, *Thin Solid Films* 488 (2005) 15.
- [33] R. Cabala, V. Meister, K. Potje-Kamloth, *J. Chem. Soc. Faraday Trans.* 93 (1997) 131.
- [34] Joint Committee on Powder Diffraction Standards, *Powder Diffraction File No. 36-1451, 72-1464, 24-1470, and 41-1445*.
- [35] D.J. Qiu, H.Z. Wu, A.M. Feng, Y.F. Lao, N.B. Chen, T.N. Xu, *Appl. Surf. Sci.* 222 (2004) 263.
- [36] D. Tsiulyanu, S. Marian, H.D. Liess, I. Eisele, *Sens. Actuators, B* 100 (2004) 380.
- [37] M.J. Madou, S. Roy Morrison, *Chemical Sensing with Solid State Devices*, Academic Press, Inc., Boston, 1989, p. 556.
- [38] A. Bielanski, J. Haber, *Oxygen in Catalysis*, Marcel Dekker, New York NY, 1991.
- [39] W.H.G. Horsthuis, *Thin Solid Films* 137 (1986) 185.
- [40] P. Clifford, D. Tuma, *Sens. Actuators* 3 (1983) 233.
- [41] C.C. Wang, S.A. Akbar, M.J. Madou, *J. Electroceram.* 2 (1998) 273.
- [42] Y. Takao, K. Miyazaki, Y. Shimizu, M. Egashira, *J. Electrochem. Soc.* 141 (1994) 1028.